Molecular BioSystems

Accepted Manuscript

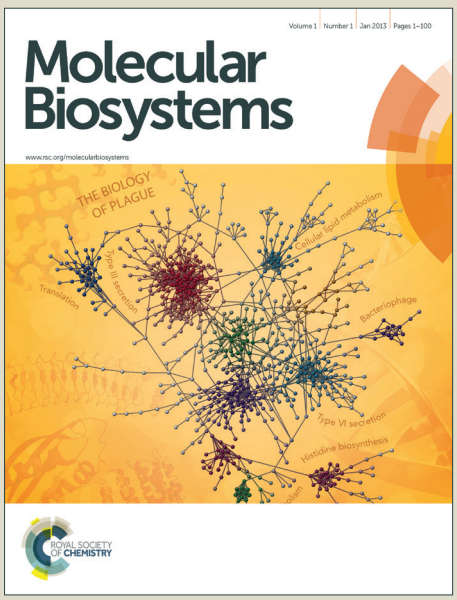

ROYAL SOCIETY OF CHEMISTRY

www.rsc.org/molecularbiosystems

Journal Name

RSCPublishing

ARTICLE

Design of dual inhibitors of ROCK-I and NOX2 as potential leads for the treatment of neuroinflammation associated with various neurological diseases including autism spectrum disorder

Cite this: DOI: 10.1039/xoxxooooox

Received ooth January 2012,
Accepted ooth January 2012

DOI: 10.1039/xoxxooooox

www.rsc.org/

Reshma Alokam[a], Sarthak Singhal[a], Geetha Sai Srivathsav[a], Sowmya Garigipati[a], Sripriya Puppala[a], Dharmarajan Sriram[a] and YogeeswariPerumal[a]†

Inhibition of both Rho kinase (ROCK-I) and NADPH oxidase (NOX2) to treat neuroinflammation could be very effective in the treatment of progressive neurological diseases like Alzheimer's disease, autism spectral disorder, and fragile X syndrome. NOX2 being a multi-enzyme component is activated during host defense in phagocytes such as microglia, to catalyze the production of superoxide from oxygen, while ROCK is an important mediator of fundamental cell processes like adhesion, proliferation and migration. Phosphorylated ROCK was found to activate NOX2 assembly via Ras related C3 botulinum toxin substrate (Rac) in disease conditions. Overexpression of ROCK-I and NOX2 in innate immune cells like microglial cells contribute to progressive neuronal damage early in neurological disease development. In the present study we employed computer-aided methodology combining pharmacophore and molecular docking to identify new chemical entities that could inhibit ROCK-I as well as NOX2 (p47 phox). Among the huge dataset of a commercial database, top 18 molecules with crucial binding interactions were selected for biological evaluation. Seven among the lead molecules exhibited inhibitory potential against ROCK-I and NOX2 with IC_{50}s ranging from 1.588 to 856.2 nM and 0.8942 to 10.24 μM respectively and emerged as potential hits as dual inhibitors with adequate selectivity index (SI= CC_{50}/GIC_{50}) in cell–based assays. The most active compound **3** was further found to show reduction of the pro-inflammatory mediators such as TNFα, interleukin-6 (IL-6) and interleukin-1beta (IL-1β) mRNA expression levels in activated (MeHg treated) human neuroblastoma (IMR32) cell lines. Hence the present work documented the utility of these dual inhibitors as prototypical leads to be useful for the treatment of neurological disorders including autism spectrum disorder and Alzheimer's disease.

Introduction:

Neuroinflammation constitutes as primary hallmark in the progression of various neurological diseases including Alzheimer's, multiple sclerosis, autism spectrum disorder (ASD), etc. [1-3]. Autism spectrum disorder is one of the severe neurodevelopmental disorders with high variability in its clinical representation. Recent studies have implicated oxidative stress, mitochondrial dysfunction and neuroinflammation to be interlinked to ASD [4]. It has also been reported that neuroinflammation is associated with neurodegenerative disorders- both acute and chronic. In this context, microglial cells seem to play a crucial role and therefore microglia and cytokines have been extensively studied in these conditions [5]. With the growing interest in the role of reactive oxygen species (ROS) in cell biology, the significance of its connection with neuroinflammation is becoming progressively clearer. NADPH oxidases are dedicated enzymes for the generation of ROS via reduction of molecular oxygen and have been the major contributor to brain injury and neuroinflammation in various neurological disorders [6-7]. Rho GTPases are one of the five families of the Ras super family. Members of the Rho GTPase family like Rho kinase and Rac have been found to play a central regulatory role in NOX (p47 phox) activity. Newey and Kasri *et.al* reported on Rho GTPases being involved in the dendrite development that are important for cognition. Altered spine morphology and synaptic activity have been linked with cognitive disabilities and mental retardation wherein Rho GTPase has emerged as key regulator of actin and microtubule cytoskeletons [8,9]. A link between Rho GTPases and reactive oxygen species (ROS) [10] has been shown. In line with the growing interest in the role of ROS in cell biology, the relevance of this connection is becoming increasingly clearer. ROCK had been reported to be interlinked with NOX, wherein Rho GTP and Rac

proteins upon activation bind to p67 phox subunit which further bind to p40 and p47 phox to complete the cytosolic subunit assembly of NOX isoforms [11-12]. Based on these literature evidences as both ROCK-I and NOX2 pathways being involved in neurite outgrowth and retraction and with the growing interest in Alzheimers, ASD, and other related neurological diseases, inhibition of ROCK-I and NOX2 (p47 phox) seem to be attractive pharmacological targets for the treatment of neuroinflammation. Hence in the present study, we utilized structure-based design strategy involving energy-based pharmacophore and shape-based modeling to identify dual inhibitors of ROCK-I and NOX2 (p47 phox) and report the bioevaluation results.

Materials and methods:

Target structure preparation:

In this study, we utilized crystal structures of ROCK-I (PDB code: 2ESM) bound to fasudil and NOX2, (PDB code: 1OV3) whose p47 phox subunit bound to proline rich region of p22 phox (peptide). The 3D coordinates of these enzymes were obtained from PDB and processed further by removing all the water molecules as well as other heteroatoms except the bound inhibitor or peptide in both structures. Hydrogens were added to the target protein by OPLS_2005, and further minimized using Impref. The resultant target proteins were used in molecular docking studies.

E-pharmacophore and Shape Generation:

The prepared protein was used as an input file for generating the receptor grid file, and for docking simulations. During docking simulation using different module of Schrodinger, potential of non-polar parts of ligands was softened by scaling van der Waals radii of ligand atoms by 0.8 with partial charge cutoff of 0.15. During docking simulation, Glide [12] was employed for redocking and generation of grids. The docking simulation was performed by allowing flexible torsions in ligands with the use of XP (extra precision) mode, highly robust and very accurate. The parameter selected for docking run was default and a model energy function named glide score (Gscore) was used which combined the force field and empirical terms for selecting best docking pose, generated as output. Glide XP descriptors include terms for hydrophobic enclosure, hydrophobically packed correlated hydrogen bonds, electrostatic rewards, π-π stacking, π-cation, and other interactions. ChemScore, hydrogen bonding and lipophilic atom pair interaction terms are included when the Glide XP terms for hydrogen binding and hydrophobic enclosure are zero.

E-pharmacophore Generation: Receptor Grid Generation tool in Maestro software package was used to generate energy grids for all prepared protein structures. A hybrid approach of ligand and structure based techniques which employ docking energy score for finding the bio-active compound against the receptor was utilized for the generation of energy-based pharmacophore. The procedure followed was as reported earlier by our group [14]. Pharmacophore sites were automatically generated with Phase (Phase, v3.0, Schrodinger, LLC, New York, NY) using the default set of six chemical features: hydrogen bond acceptor (A), hydrogen bond donor (D), hydrophobe (H), negative ionizable (N), positive ionizable (P), and aromatic ring (R). Hydrogen bond acceptor sites were represented as vectors along the hydrogen bond axis in accordance with the hybridization of the acceptor atom. Hydrogen bond donors were represented as projected points, located at the corresponding hydrogen bond acceptor positions in the binding site. Projected points allow the possibility for structurally dissimilar active compounds to form hydrogen bonds to the same location, regardless of their point of origin and directionality. Each pharmacophore feature site was first assigned an energetic value equal to the sum of the Glide XP contributions of the atoms comprising the site, allowing sites to be quantified and ranked on the basis of the energetic terms.

Shape Generation: ROCS (Rapid Overlay of Chemical Structures), a shape based method for rapid similarity analysis of molecules was employed in this study. The volume overlap of molecules was assessed by Gaussians, which were parameterized according to the hard sphere volume of heavy atoms. The use of Gaussians allowed for fast calculation of overlaps between two atoms. ROCS considered both shape and a color force field for optimization of the overlap. The basic scoring function implemented in ROCS was the shape tanimoto score, which was a quantitative measure for the shape overlap of two molecules. In order to obtain activity on our target proteins, not only shape but also appropriate chemical functionality was crucial and using ROCS implemented color score supported the alignment process and evaluated chemical feature based similarity [14, 15]. The ROCS color force field was composed of SMARTS patterns for the characterization of chemical functions in combination with a rule set. ROCS provided two color force fields, Implicit Milis Dean and Explicit Milis Dean force fields. As the Implicit Milis Dean force field included a basic pKa model assuming pH 7, charges were assigned accordingly in an automated way, and users need not protonate molecules accordingly before virtual screening. ComboScore function with equal weights on its both components, the ShapeTanimoto and the ScaledColoreScore was utilized. Overall, this screening and scoring approach was straightforward, based on a few basic assumptions, and as also observed with related techniques like e.g.; pharmacophore modelling [15].

Docking studies:

Glide performed an exhaustive search employing hierarchical filter for finding most favorable interaction between one or more ligand molecules and the proteins. Receptor-grid files were generated after preparing correct forms of proteins and ligands using receptor grid generation program. For grid generation potential of non-polar parts of receptor was softened by scaling van der Waals radii of ligand atoms by 1 Å with partial charge cutoff of 0.25. Glide module had three types of docking, high through put virtual screening (HTVS), standard precision (SP) and extra precision (XP) mode. The XP mode was used for exhaustive sampling and advanced scoring,

resulting in higher enrichment. Finally we identified top ranked molecules based on docking score and visual inspection.

Expression and Purification for ROCK1:

pET21(+)-ROCK-I recombinant obtained from NII, New Delhi (India) was transformed into *E. coli* BL21 (DE3) for ROCK-I production based on IPTG induction. Transformed cells with recombinant BL21 (DE3) were grown in LB medium supplemented with 50 µg/ml of kanamycin and incubated at 37^{0}C on shaking incubator with 150 RPM to an A600 ≈0.6. Protein synthesis was induced with 0.1 mM IPTG at 18^{0}C overnight. Induced cells from culture of BL21 (DE3)/pET21(+)-ROCK-I recombinant (300mg of cells) was suspended in lysis buffer (137mM NaCl, 2.7mM KCl, 10mM Na2HPO4, 1.8mM KH2PO4, 1mM DTT, protease inhibitors cocktail and 5% Glycerol). The cell suspension was sonicated for 12-15 cycles (20s pulse and 45s halt) and centrifuged at 8000rpm at 4^{0}C for 10minutes. Repeated centrifugation of supernatant with 10000 rpm at 4^{0}C for 35mins yielded clear lysate. Pre-equilibration of the clarified lysate with Ni-NTA resin for 3.30 h at 4^{0}C was performed. Centrifugation of whole content at 500 rpm for 5 min at 4^{0}C was done and removed the supernatent as much as possible and loaded the pre-equilibrated beads on to column. The column was equilibrated with lysis buffer and wash buffer (500 mM NaCl, 2.7 mM KCl, 10 mM Na_2HPO4, 1.8 mM KH_2PO4, 1 mM DTT, 1 mM PMSF and 5% Glycerol), each for 10 min and centrifuged for 5 min at 4^{0}C. Protein bound beads were washed with elution buffer (140 mM NaCl, 25 mM Tris-Cl (pH 8.0), 1 mM DTT, 1 mM PMSF, 5% Glycerol and 200 mM Imidazole). The eluted protein was finally concentrated upto 3 mg/ml.

ROCK enzyme inhibition studies:

Reaction volumes of 100 µM of myelin basic protein (MBP Sigma-Aldrich Co. LLC) and 20 pM of ROCK-I enzyme in 0.1 M HEPES (pH 7.6), 10 mM $MgCl_2$, 2.5 mM PEP, 0.2 mM NADH, 0.03 mg/ml PK (pyruvate kinase), 0.01 mg/ml LDH (lactate dehydrogenase), 2 mM DTT, and inhibitors at different concentrations (100µM-0.001µM) were incubated at 25^{0}C for 10 min. The reaction was initiated with 30 µM of ATP and proceeded at 25^{0}C for 5 min. Progress of reaction was monitored as a function of time by the decrease in absorbance at 340nm due to the oxidation of NADH [16].

Thermofluor Assay for ROCK:

The stabilization of top active leads when bound to protein was evaluated by thermal shift assay, where the native protein ROCK-I and protein-ligand complexes were subjected to gradual temperature rise in the presence of fluorescent dye Sypro orange (Sigma Aldrich). The fluorescence emitted from the dye was a measure of protein denaturation, where the hydrophobic residues were exposed [17]. Sypro orange fluorescent dye (Sigma-Aldrich Co. LLC) supplied as a 5000X solution in 100% DMSO was utilised. First, the dye was diluted in 100 mM HEPES buffer to a concentration of 10X before adding to the protein, to prevent damage of protein with high concentrations of DMSO. 100 µg/ml of ROCK-I protein solution with 1µM of inhibitor (total DMSO concentration is <0.1%) and diluted sypro orange to a total volume of 30 µl was taken. Reference control wells (no ligand wells) containing the appropriate amount of DMSO were distributed on 96-well plate. Plate was stepwise heated from 25^{0}C to 95^{0}C to obtain T_m values. As the temperature was increased, the stability of the protein decreased and become zero at equilibrium where the concentrations of folded and unfolded protein were equal and this temperature was defined as melting temperature (T_m). The shift in the melting temperature of protein in presence of ligands was observed.

Cell viability assay:

Human embryonic kidney epithelial cells (HEK 293) were procured from NCCS, Pune (India). The cells were further grown in RPMI-1640 supplemented with 10% FBS, 100 IU/ml penicillin and 100 µg/ml streptomycin and maintained at 37^{0}C in 5% CO2 by standard cell culture techniques. After culture of HEK 293, (5.0×103 cells/well) in a 96-well p-lysine coated flat bottom plate (NEST Biotechnology Co.Ltd) supplemented with RPMI-1640 (200µl) different concentrations of compounds (100 µM-0.01µM) were incubated for 48 h. After incubation, 20 µl/well of (3-(4,5-dimethythiazol-2-yl)-2,5-diphenyl tetrazolium bromide (MTT) solution (5mg/ml in phosphate buffered saline pH 7.4) was added to cells and then incubated for additional 3 h at 37^{0}C under 5% CO2. The medium was removed from wells and dissolved with MTT crystals (200 µl/well) and the absorbance was determined at 570nm using spectrophotometer [18] (SpectraMax M4, Molecular Devices, Sunnyvale, USA).

Methymercury induced cell-based assay:

Human neuroblastoma cell lines (IMR-32) were purchased from NCCS, Pune (India). The cells were grown in T25 flasks (NEST Biotechnology Co.Ltd) supplemented with MEM (10% FBS, 100 IU/ml penicillin and 100 µg/ml streptomycin) for 24 h. After attainment of 100% confluence, (5.0×103 cells/well) there were taken in 96-well p-lysine coated flat bottom (NEST Biotechnology Co.Ltd) plates supplemented MEM (200µl) for 2 h in presence of different concentrations of compounds (100 µM-0.01 µM) and followed by 10 µM MeHg (Sigma-Aldrich Co. LLC) treatment for 3 h and the cells were further allowed to grow for 48 h. After incubation, MTT was added same as above for all wells to estimate the absorbance [19].

Intracellular X-ROS estimation:

Intracellular ROS estimation was measured using DCFH-DA [20]. Approximately 5000 HUVEC cells (NCCS, Pune, India) per well were plated in 96 well plate, treated with 5 µM DCFH-DA for 1hr followed by 20 µg lipopolysaccharide (LPS) for 2 h. Compounds were added at varying concentrations for 3h, fresh medium replenished and cells cultured further for 24 h. Oxidized DCFH excitation and emission was measured at 485 and 525nm respectively in a spectrophotometer (SpectraMax M4, Molecular Devices, Sunnyvale, USA). Fasudil was employed as a positive control. Percent ROS production inhibition was calculated using GraphPad prism 5.03.

Clonogenic assay:

Clonogenic assay was performed according to the method reported by Puck and Marcus [21]. The experiment was carried out by seeding approximately 1000 IMR-32 cells per well in 6 well plate. The optimum concentration of 10 µM of MeHg was selected from previous experiment; cultures were treated in as MeHg alone for 3h. For compounds, cultures were treated with 1 µM of compound for 2 h before treating with MeHg for 3 h [22]. After various treatments, MeHg and compounds containing media were discarded and fresh MEM media was added and the cultures were left undisturbed for 14 days at 37^0C in 5% CO2 incubator for colony formation and the colonies were washed with 1XPBS followed by staining with 0.5% gentian violet in methanol. After 30 min, slowly rinsed off the stain without disturbing colonies and washed with tap water later and allowed it to air dry. The plating efficiency and survival fraction were calculated as follows,

Plating efficiency $PE = \frac{No.Of\ Colonies\ formed}{No.Of\ cells\ seeded} X100$

Survival fraction $\boldsymbol{SF = \frac{No.Of\ colonies\ formed\ after\ treatment}{No.Of\ cells\ seeded\ X\ PE}}$

Cell motility studies:

For measuring cellular motility, 105 IMR-32 cells were plated on 6well p-lysine coated plates (NEST Biotechnology Co.Ltd) supplemented with MEM for 2 h in presence of test compound and fasudil at 1 µM and followed by 10 µM MeHg (Sigma-Aldrich Co. LLC) treatment for 3 h. Using a sterile pipette tip (10 µl), cell monolayer was scratched vertically to make a wound. The cells were rinsed with 1X PBS and replaced with 1.5 ml of supplemented MEM [22]. Images were captured taken at 0 h and 24 h using 10X magnification with an inverted microscope (OLYMPUS IX53).

RNA isolation and Real Time Quantitative PCR studies:

10^5 IMR-32 cells in 35 mm petridish were treated with MeHg for 3 h followed by 1 µM test compound for 2 h. Cells were trypsinised and centrifuged at 5000 rpm for 3 min. The cell pellet was taken and total RNA was isolated using TRIzol reagent (Sigma-Aldrich Co. LLC) according to the manufacturer's instructions. Transcript levels of inflammatory mediators like IL-6, IL-1β and TNFα were assessed using BIO-RAD CFX Connect Real Time System (BIO-RAD Laboratories, Inc). 1 µg of total RNA was used as a template to make the first strand cDNA by Anchored oligo dT priming with a commercial cDNA synthesis kit (Verso cDNA synthesis kit, Thermo Fischer scientific, Inc). Real time PCR was performed according to the manufacturer's instructions using a BIO-RAD CFX Connect with SYBR green (Kapa Biosystems) as the fluorescent dye enabling real-time detection of PCR products. The synthetic gene specific primer sets used in PCR were (1) IL-6 forward primer: 5'-TTCGGTCCAGTTGCCTTCTC-3'; reverse primer: 5'-GAGGTGAGTGGCTGTCTGTG-3'; amplicon size is 122bp (2) IL-1β forward primer: 5'- GCAAGGGCTTCAGGCAGGCCGCG-3'; reverse primer: 5'- GGTCATTCTCCTGGAAGGTCTGTGGGC-3'; amplicon size is 96bp (3) TNFα forward primer: 5'-CTCCAGGCGGTGCCTTGTTC-3'; reverse primer: 5'-CAGGCAGAAGAGCGTGGTG-3'; amplicon size is 100bp [22, 23] (4) ROCK-I forward primer: 5'-GAAGAAAGAGAAGCTCGAGAGAAGG-3'; reverse primer: ATCTTGTAGCTCCCGCATCTGT-3'; amplicon size is 369bp [24] (5) CRMP2 forward primer: 5'-AGACATATACATGGAAGATGGGTT-3'; reverse primer: 5'-CCATACACCACAGTTCCCTTCT-3'amplicon size is 729bp [25] and (6) GAPDH forward primer: 5'-GGAGTCCACTGGCGTCTT-3'; reverse primer: 5'-AGGCTGTTGTCATACTTCTCAT-3' amplicon size is 100bp [23, 27]. All samples were run in triplicates and the output level was reported as the average of three cells. The cycle conditions were 94^0C for 3 min, followed by 45 cycles of 94^0C for 30s, 62^0C for 30s and 72^0C for 60s. For quantification, the target gene was normalized to the internal standard GAPDH gene.

Statistical analysis:

Results are expressed as the means and SEM. Multi group comparison was performed by one-way analysis of variance, followed by the Tukey's Multiple Comparison Test as a post hoc analysis. Calculations were performed using GraphPad Prism program software (GraphPad Software, San Diego, CA).

Results and Discussion:

The pharmacophore modelling procedure, which has been a great success in medicinal chemistry, was utilized in this study. Two different pharmacophore modelling approaches have been widely used in computer-aided drug discovery research. Pharmacophore model could be based on a set of ligands with experimentally known inhibition for a particular therapeutic target or could be exploited from the receptor-based information. Our strategy was based on the information extracted from the protein bound with the ligand to identify dual inhibitors of ROCK-I and NOX2. As a first step, e-pharmacophores were generated for both the target proteins using their crystal structure bound to inhibitor and substrate for ROCK-I and NOX2 respectively. The second step involved virtual screening of the commercial database (Asinex) to map over the derived pharmacophore models and finally was docked into both the two target proteins (Figure 1). Compounds were shortlisted based on their docking scores. E-pharmacophore and shape was generated based on the interaction profile of the peptide-5 with the p47 phox SH3 domain. E-pharmacophore and shape models are presented in Figure 2. All the calculations were done in Schrodinger and Openeye systemic software for e-pharmacophore and shape respectively. Features of e-pharmacophore were very well matched with the shape. For ROCK-I e-pharmacophore and shape models were generated using 2ESM PDB coordinates which was bound to fasudil as shown in Figure 2.

The crystal structure of SH3 domain of p47 phox bound to proline rich region of p22 phox (a 10 amino acid peptide) was employed (PDB code 1OV3). As the bound inhibitor was a decapeptide (Peptide-1, Table 1) we truncated and analysed for docking as our major objective was to identify small molecules. To preclude these compounds, the decapeptide was spliced into small fragments and prepared using Ligprep and docked into the grid to check the RMSD of the docked pose (Table 1). Reproduction of the crystal pose conformation of the peptide was a minimum requirement to

determine whether a docking setup was effective. The peptide-5 was found to exhibit good docking score and was able to reproduce the interactions shown by parent peptide-1. Thus peptide-5 was chosen for further generation of e-pharmacophore and shape-based models. E-pharmacophore was generated for this peptide of p22 phox (PPPRPP) which exhibited highest docking score and RMSD (0.6587) when redocked into the grid generated by Glide with a maximum number of seven features. The generated e-pharmacophore is shown in Figure 2 energy scores with two acceptors A2 (score-0.67) and A4 (score-0.60) together with two positive ionisable groups namely P15 and P16 with scores -2.87 and 0.00 respectively. We employed 3 feature pharmacophore for mapping hit compounds from a large library of commercial database (Asinex) and molecular docking with p47 phox.

Further shape modeling was also generated for the same peptide using vROCS. Query validation was not possible as there were no reported inhibtors for NOX2 assembly. The query was able to reproduce the same features which were present in crystal ligand interactions. Amino group in arginine was found to interact with the Glu244 and Asp243 (supporting information Figure S3) of p47 phox, which was depicted as donor feature in query. Carboxyl group of second proline at N-terminal end interacted with Trp263 of p47 phox, which was depicted as donor group in query. Looking at these features many of them were in agreement with the e-pharmacophore generated using Glide (Figure 2). Comparison of e-pharmacophore and shape generated features revealed a clear cut similarity in number of features of acceptors, positive ionisable sites and hydrophobic groups, but e-pharmacophore contains donors in place of positive ionisable sites in shape. This may be due to the selection of different algorithms. This suggested and supports our predictions regarding the minimum features required in ligand molecule to behave as NOX2 assembly inhibitors and helpful in screening large database as future anti-inflammatory agents.

The pharmacophore model for ROCK-I was built using crystal structure of fasudil in complex with ROCK-I [28,29]. Aromatic ring in fasudil showed more affinity towards the hydrophobic pocket and amino group was bound specifically to Met156 [30] residue in the active site of ROCK-I. The experimental inhibitory value of fasudil was approximately 1μM. Fasudil exhibited a docking score of -7.521 with a maximum number of four features at the binding site. The generated e-pharmacophore is shown in Figure 2 with one acceptor required for the interaction within the pocket namely A1 (score-2.16) and two ring aromatic groups namely R7 and R8 with energy scores -2.98 and -0.99 respectively. A three feature pharmacophore model was used for mapping the database compounds. Similarly shape was generated for the same crystal ligand using vROCS.

The reliability of the generated pharmacophore models were validated on the basis of the presence of chemical features necessary to interact with key amino acid residues in the active site of the corresponding target protein. The pharmacophore model generated for the ROCK-I inhibitors was found to possess the required features that were complementary to the active site. Thus pharmacophore was mapped with a set of 20 already reported inhibitors for the ROCK-I and 1000 non drug like molecules collected from Schrodinger decoy sets. Enrichment factor (EF) was employed for the fraction of known actives recovered when a fraction of database was screened. A decoys containing set of 1020 molecules mentioned above were used to calculate the EF. For this, we focused on EF (1%) which was the enrichment in the top 1% of the decoys. A second enrichment used was BEDROC (Boltzmann–enhanced discrimination of receiver operating characteristic) to ensure that the results and conclusions were significant. We used α=20.0 which paralleled to 80% of the score being accounted in the top 1% of the database. A second enrichment for the shape employed was the AUC (area under curve) which was found to be 0.984 and was indicative of a query that was predictive and was able to separate the actives from decoys . For p47 phox pharmacophore models there were no known NOX2 assembly inhibitors reported and thus the validation for these was not done. The EF 1% value was found to be 59 and was a good indication that ROCK-I e-pharmacophore model could be useful to identify actives with the BEDROC (α=20.0) of 0.816. In case of ROCK-I shape AUC was 0.984 and EF 1% was 77.68 [31] EF is calculated using the following formula.

$$EF = \frac{(H_a \times D)}{(H_t \times A)}$$

Asinex, a commercial database containing 500000 diverse chemical compounds, was screened using various drug-like parameters in order to remove the non-drug like compounds. LigPrep (LigPrep, version 3.0, Schrödinger, LLC, New York, NY, 2014) module available in Schrodinger was used to prepare the database. LigPrep removed all duplicate structures as well as generated 3D conformation using OPLS_2005 force field and Impref minimization. Finally, the large database compounds were used subsequently in pharmacophore mapping. Advanced pharmacophore screening was used to map all the hit compounds for both pharmacophore models of p47 phox and ROCK-I. All molecules were mapped on to the pharmacophore with the fitness set to =1.00, alignment score 1.2, volume score 1.0 and vector score 1.0. These compounds were also subjected to a simple ROCS run option with ImplicitMillsDean force field to map all hit compounds to shape model. Out of 10000 hit compounds, 6000 compounds were found to be well mapped onto the shape model of fasudil. These were further selected based on their fitness (> 1.5) which yielded 120 molecules and after tanimoto combo (>0.8) resulted in 100 molecules.

The hit compounds obtained from the ligand mapping experiment performed for ROCK-I and NOX2 inhibition from the Asinex database mapped onto respective pharmacophores were used for docking experiment. The prepared p47 phox stucture was employed to screen these hits using Glide module. The compounds from the pharmacophore filtering were docked into the active site defined by the peptide-5. All the hits were successfully docked without any error during post dock minimization. The crystal ligands exhibited Glide g score of -6.265 for peptide-1 and -7.593 for peptide-5. The top 1000 hit compounds from database scoring whose Glide g score were less than -6.0 were retained as possible p47 phox inhibitors. In order to obtain dual inhibitors of p47 phox and ROCK-I, the final hits obtained from p47 phox docking was examined for their affinity for ROCK-I. The coordinates of the prepared crystal structure of ROCK-I which was devoid of water molecules and other heteroatoms except the bound fasudil was utilized as second target in molecular docking experiment. The active site was defined by fasudil grid with the radius of 20 Å was employed. The hits that mapped well on both target's pharmacophore models were used as

ligands. All other parameters were kept at the same values as used in molecular docking for the p47 phox enzyme. The compounds from the pharmacophore filtering were docked into the defined active site around the fasudil.

The binding modes of all the docked compounds were analyzed for their molecular interactions at the active site. On the basis of the commonality on both targets, binding mode analysis and structural diversity, finally eighteen compounds (Figure 3 and Supporting Information Figure S1) with good binding characteristics were shortlisted as possible dual inhibitors for these enzyme targets that were involved in neuroinflammatory process. The docking score and hydrogen bond information are presented in Table 2 and supporting information Table S1 for all 18 compounds. These 18 compounds exhibited crucial hydrogen bonding with Met156 in ROCK-I and Ser208 hydrogen bonding in p47 phox (Table 2). The pharmacophore fitness and tanimota coefficient of all the 18 compounds are presented in supporting information Table S2. Human ROCK-Iwas cloned as N-HIS6-tagged protein using pET 21(+) vector. ROCK-I (N-HIS6 tagged) protein was expressed as soluble forms in *E. coli* BL21(DE3) cells by induction with isopropyl-1-thio-b-D-galactopyranoside (IPTG, 0.1 mM). This was easily purified using Ni2+ -affinity chromatography. The expression level of soluble and active N-HIS6 tagged proteins was relatively higher. About 3 mg of N-HIS6 tagged proteins was routinely obtained from the cell lysate of 1 l *E. coli* cell culture. Sodium dodecylsulfate–polyacrylamide gel electrophoresis (SDS-PAGE) analysis indicated that one step Ni2+ -column purification was sufficient as it provided pure ROCK-I. As expected from the calculated molecular weight of N-HIS6 tagged ROCK-I, the size of the protein shown by SDS-PAGE was about 158 kDa.

Having identified the hit molecules from *in silico* screening approach, we hypothesized that the designed compounds would possess the ability to bind with ROCK-I and consequently inactivate its activity. To test this hypothesis, the compounds were initially screened for ROCK-I enzymatic activity. The compounds were screened at different concentrations from 100 µM-1 nM employing the standard ROCK-I enzyme assay protocol [19] and relative inhibition of ROCK-I activity was evaluated for IC_{50} calculations. Among the tested compounds three of them (**1-3)** displayed least IC_{50}s (1.848, 1.588 and 1.879 nM respectively) against ROCK-I enzyme. Other compounds that exhibited showed comparatively weak inhibition of ROCK-I were **6** and **7** that displayed IC_{50} of 21.58 nM (Table 2). The docking pose displaying the interaction profile of compound **3** with ROCK-1 and NOX2 has been presented in supporting information Figure S2.

ROCK signaling pathway was previously reported to increase cell viability in few cell types, while enhancing apoptotic pathways in few other cell lines. The mechanism behind this noticeable ambiguity was unknown. To conclude the role of ROCK signaling pathway in cell survival, Catherine *et al.* [32] treated various neuroblastoma cells with cisplatin, UV, hydrogen peroxide and also with novel ROCK-I inhibitor, Y27632 and measured the cell survival 72 h post treatment. The results showed that pharmacological inhibition of ROCK-I led to significant increase in cell survival among all treatments. Hence this prompted us to investigate the ROCK-I inhibitors in cell based assays in vitro. Previous studies have demonstrated that inhibition of the Rho/ROCK pathway prevented MeHg-induced intoxication of neuronal cells [33]. In another study, MeHg exposure down-regulated the expression of Rac1 and RhoA causing axonal degeneration and apoptosis of cultured cortical neuronal cells [34]. In this present study, we therefore utilized IMR-32 neuroblastoma cells treated with MeHg, as model to evaluate the effect of the eight ROCK-I inhibitors. The compounds were also analyzed in cell based assays for their cytotoxicity parameters. Addition of MeHg to IMR32 elevated expression of ROCK-I (Figure 4). In this system test compounds were able to reduce the cell proliferation in a dose dependent manner and their GIC_{50} values ranged from 3 nM to 33 µM. The dose dependent suppressive effect of compounds on cell proliferation was accompanied by a marked decrease in ROCK-I and CRMP2 expressions. In HEK 293 system, compounds displayed no cytotoxicity and the CC_{50} values ranged from 1.15 µM to 428.2 µM. Thus selectivity index ($SI=CC_{50}/GIC_{50}$) was calculated to obtain a selectivity index. The SI of compound **3** was found to be the highest (Table 2) which was due to its lesser toxicity and more therapeutic capacity. Whereas compound **1** showed a minimal SI of 0.0344, which was deterrent due to high toxicity compared to bioactivity. Other compounds SI was found in the range from 2.4 to 28.8. The antiproliferative activity of these compounds was also evaluated using the clonogenic assay. Clonogenic assay was an effective method for the determination of single cell proliferation capacity, thereby indicating the reproductive ability to form a large colony or clone. Clonogenic assay has been reported as the method of choice to determine cell reproductive death after treatment with cytotoxic agents to determine their effectiveness [35]. We found that IMR32 cells were able to form colonies in response to exposure to test compounds compared to those without any treatment. In this assay, compound **3** (SF= 5.776) was found to produce significant number of colonies compared to control and fasudil (SF= 3.136) treated systems. Expression of ROCK-I was significantly decreased in compound **3** treatment at 1µM concentration, whereas CRMP2 activity was reduced slightly (Table 2).

Compound **3** being the most promising lead based on ROCK-I inhibition, SI and clonogenic potency, we undertook biophysical characterization of the compound **3** using themofluor assay to assess the stability of the ROCK-I protein upon ligand binding. The temperature, at which protein melts (T*m*), is a measure of protein stability. Thermal shift assays have many biophysical attributes that satisfy the requirements of a general cross target drug discovery assay. Ligand induced conformational stabilization of protein has been a well understood phenomenon in which substrates, inhibitors, cofactors, metal ions, synthetic analogues of natural ligands and even other proteins provide enhanced stability to proteins on binding. This phenomenon was based on the energetic coupling of the ligand binding and receptor melting reactions. This energetic linkage result in ligand-dependent changes in the midpoint for thermally induced melting curves for the ligand receptor complex relative to the uncomplexed receptor (ΔT_m) [36]. The results from the miniaturized thermal shift assay using differential scanning flurometry were found to correlate with the results obtained through the enzymatic assay by the reasonable fit to the slope for temperature Vs RFU (10^3). Data analysis for this experiment was simplified

using CFX manager V3.0 software that displayed the computed T_m determinations for all wells. The results for the blank (red peak, Figure 5) which was only enzyme with the dye showed T_m of 40.20^{0}C, whereas compound **3** (blue peak, Figure 5) in complex with enzyme showed T_m of 43.30^{0}C. Usually the T_m shift more than 1 could be considered as strong binding to the receptor. Thus compound **3** with a T_m shift of +3.30^{0}C at 1μM concentration was an indication that it had interacted with the enzyme effectively.

Cell migration is a complex phenomenon that requires coordination of numerous cellular processes. Rho kinase, mainly promote myosin II activity by inhibiting the myosin light chain (MLC) phosphatase and phosphorylating myosin light chain. This in turn favors the assembly of actin myosin filaments that generate the tensile strength underlying the RhoA-ROCK associated dynamic events in numerous cell types [37]. Administration of ROCK-I inhibitors like fasudil was reported to induce the relaxation of these cells by suppressing myosin light chain phosphorylation and promote the cellular motility [38]. The overexpression of ROCK-I or activation of ROCK-I function by expression of constitutively active RhoA could promote MLC phosphorylation in cortical bundles [39]. In the present study, phosphorylation of MLC by ROCK-I led to invasion or cellular motility in IMR32 cells and this effect was reversed by blockade of ROCK-I function with fasudil and compound **3** as shown in Figure 6. We concluded that the motility of neuroblastoma cells was due to activation of ROCK-I function which altered the organization of MLC, as many other coordinated changes in the actin machinery were needed to drive cell motility.

X-ROS is a novel signalling pathway seen in most of the cells [40] that arises when extra cellular matter trigger local ROS production by membrane located NOX2. Human umbilical vein endothelial cell lines (HUVEC), a type of macrophages; in which NOX2 was found to be overexpressed upon stimulation with lipopolysaccharide (LPS) [40].We performed experiments to confirm the overexpression of p47PHOX in both HUVEC and IMR32 and found that in HUVEC cells the expression was more (Supporting Information Figure S3) and hence for the present study we utilized these cell lines. The physiological generation of ROS could occur as a by-product of other biological reactions in mitochondria, peroxisomes, cytochrome p-450 and other cellular elements. However, the phagocyte NOX was the first identified example of a system that could generate ROS not as a by-product, but rather as the primary function of the enzyme system. Various endogenous or exogenous inflammatory signals that alert the cells to nearby dangers were the most important biological factors that could trigger cellular NOX activation. One example was the bacterial endotoxin lipopolysaccharide (LPS), which not only activated leukocyte NOX, as expected but also showed significant effects on non-phagocytic NOX. In the present study estimation of intracellular ROS was performed using DCFH-DA. The cells treated with 10 μg/ml of LPS showed increased DCF fluorescence levels indicative of intracellular ROS production. However addition of test compounds in dose dependent manner showed dose dependent increase in DCHF oxidation as measured at 24 h (Table 2). Compound **5** showed least ROS IC_{50} of 894 nM, and compound **7** showed 964 nM. The most promising compound **3** showed ROS IC_{50} of 1.532 μM in LPS stimulated HUVEC cell lines.

The systematic study of simultaneous changes in gene expression for several pro-inflammatory cytokines in MeHg treated IMR-32 was performed using Real Time gene expression studies. Comparing the MeHg treated and untreated cells, IL-6, IL1-β and TNFα expression showed a statistically significant up regulation. Compound **3** when compared with fasudil was able to reduce significantly the expressions of IL-6, IL-1β and TNFα. However, neutralization of pro-inflammatory cytokines, especially TNFα, was clear indication of the translocation of p47 phox and p67 phox from cytosol [42]. On the other hand, over expression of TNFα and other pro inflammatory cytokines were also found to be induced by RhoA-ROCK mediated pathway [43]. The decrease in expression of inflammatory mediators by compound **3** and fasudil treated cells could be concluded to be due the possible inhibition of ROCK-I and p47 phox in MeHg treated cells as shown in Figure 4.

Conclusions

ROCK-I and NOX2 were known to have important influence on the regulation of inflammation in neurological disease progression in autism and Alzheimer's. In the present study, a strategy combining molecular docking, shape-based and pharmacophore filtering was applied to meet the critical challenges faced in designing efficient multi target inhibitors to treat complex neuroinflammatory diseases. E-pharmacophore and Shape models were developed for both the targets on the basis of the experimentally known inhibitors. Post processing of the docking results with pharmacophore filtering allowed us to bypass the difficulty with scoring functions that produce false positives from the molecular docking calculations. This pharmacophore filtering method ensured the selection of compounds with the required features. Initially, a drug like database of small molecules was prepared and docked into one of the two targets p47 phox using a widely accepted molecular docking program Glide, and the compounds with better binding characteristics were selected for further study. The compounds filtered through both pharmacophore models were docked into the active site of the second target (ROCK-I). The compounds with the better binding characteristics and with the required pharmacophore features were selected as possible dual inhibitors for ROCK-I and NOX2 enzymes to block the inflammatory signals through the ROCK-NOX pathway. Compound 3, emerged as a potential dual inhibitor that showed promising in vitro activity against ROCK-I as well as in the X-ROS estimation (LPS treated HUVEC). Further, it exhibited remarkable decrease in growth, migration and in apoptosis was better than fasudil in MeHg treated IMR-32 cell lines. In addition, there was an ameliorative change with compound **3** in comparison with fasudil against MeHg induced neurotoxicity. Results suggest that IMR-32 cells produced pro-inflammatory cytokines in response to MeHg, and further suggest that compound **3** exerted anti-inflammatory effects, at least partly by inhibiting different pro-inflammatory cytokines. Thus compound 3 could be developed as a prototypical lead to attenuate neuroinflammation in neurological disorders including ASD and AD.

Acknowledgements
We gratefully acknowledge BITS-Pilani Hyderabad Campus for providing the fellowship to one of the author Reshma Alokam and NII, New Delhi for the ROCK-I clone.

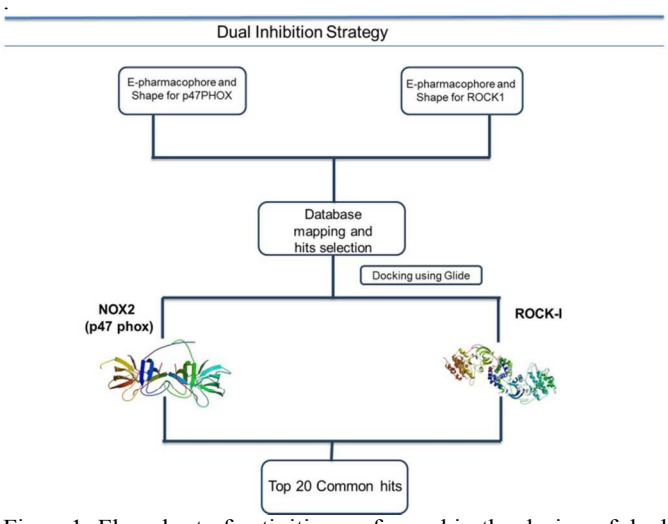

Figure1: Flowchart of activities performed in the design of dual inhibitors of ROCK-1 and NOX2 using structure-based strategies.

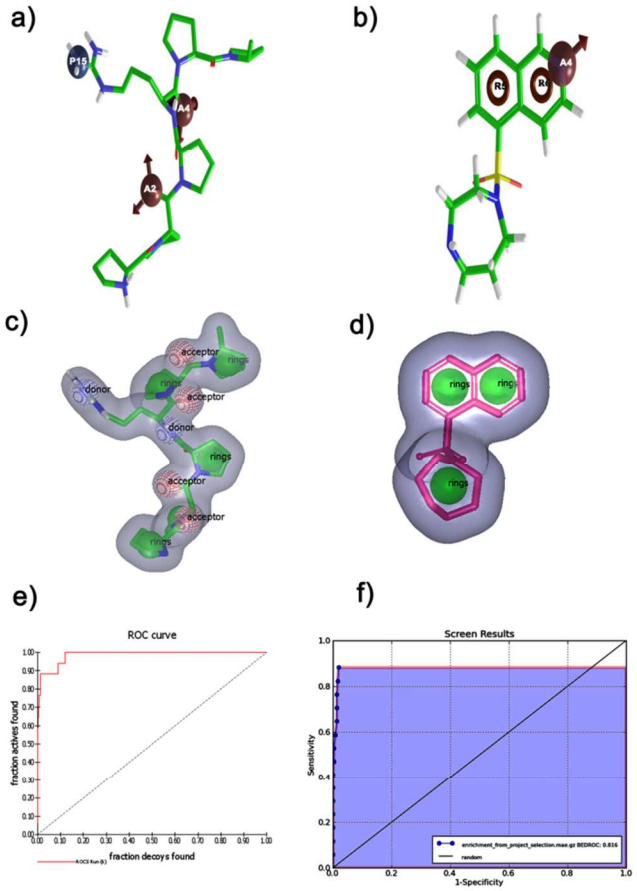

Figure2: E-pharmacophore and Shape queries employed in drug design. a) p47PHOX peptide-5 E-pharmacphore, b) ROCK1 E-pharmacophore, c) p47 PHOX peptide-5 Shape and d) ROCK1 Shape used for ligand mapping. e) ROC plot generated by vROCS during validation of ROCK1 shape. f) ROC plot of ROCK1 e-pharmacophore generated by Schrodinger, Enrichment Calculator Script.

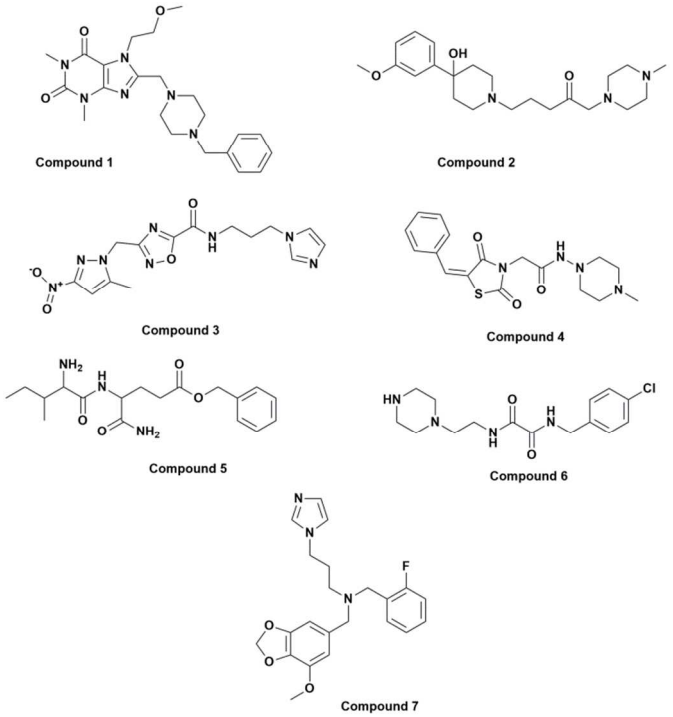

Figure3: Structures of most active 7 shortlisted hit compounds.

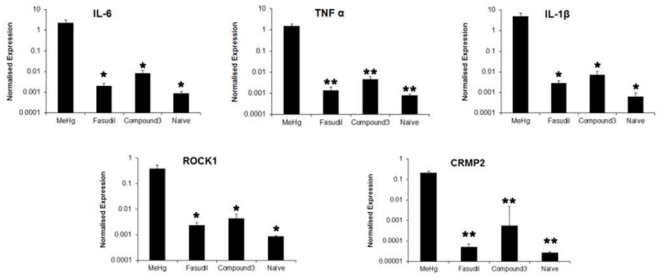

Figure4: Normalized gene expression levels of pro inflammatory cytokines, ROCK1 and its downstream substrate Collapsin Response Mediator Protein (CRMP2) in MeHg induced versus normal cells. The mRNA expression values are presented as mean±SD normalized to GAPDH levels in each sample. Y-axis values represent the number of mRNA copies relative to the number of GAPDH copies in the sample. A significant reduction of IL-6, IL-1β, ROCK1 (*P<0.01), TNFα and CRMP2 (**P<0.05) in fasudil treated cells compared to Compound **3**.

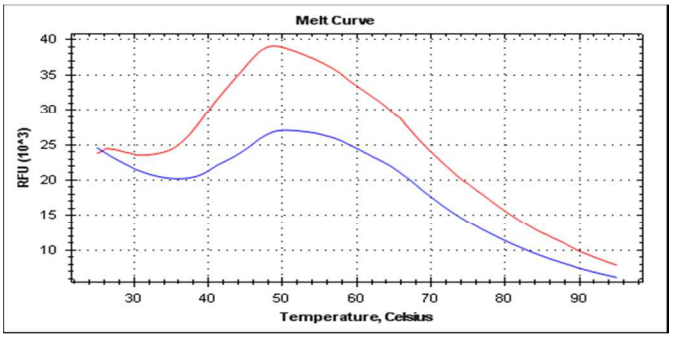

Figure5: Thermofluor assay results for ROCK1. The data were obtained for ROCK1 in the presence (Blue peak) and absence (Red peak) of Compound **3**.

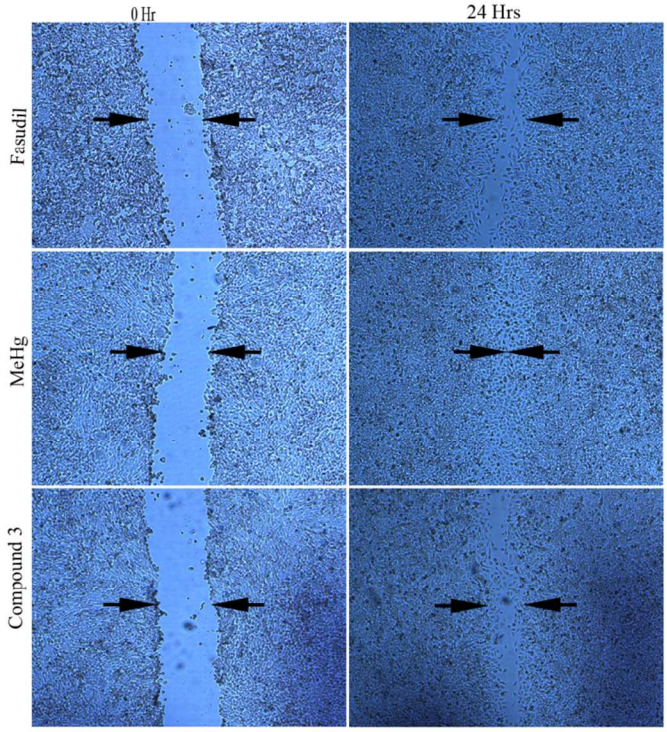

Figure6: Cell motility assay for MeHg treated IMR-32 cell lines. Migration of cells was assessed after 24h exposure to Fasudil and compound **3**.

Peptide		rmsd	Glide g Score
p22 PHOX	Peptide1	0.8915	-6.265
PSNPPPRPP	Peptide2	2.014	-5.231
SNPPPRPP	Peptide3	3.514	-6.14
NPPPRPP	Peptide4	2.621	-4.12
PPPRPP	Peptide5	0.6587	-7.593
PPPRP	Peptide6	0.826	-6.5

Table1: RMSD and docking scores of peptides of p47PHOX crystal structure.

Notes:
[a]Computer-Aided Drug Design Lab, Department of Pharmacy, Birla Institute of Technology & Science–Pilani, Hyderabad campus, Jawahar Nagar, Hyderabad–500078, Andhra Pradesh, India.
† Corresponding author: phone: +91-40-66303515; fax: +91-40-66303998; e-mail: pyogee@hyderabad.bitspilani.ac.in.

References:

[1] González, H., et al. "Neuroimmune regulation of microglial activity involved in neuroinflammation and neurodegenerative diseases." Journal of neuroimmunology (2014).
[2] Götz, J., et al. "Animal models of Alzheimer's disease and frontotemporal dementia." Nature Reviews Neuroscience 9.7 (2008): 532-544.
[3] El-Ansary, A., et al. "Neuroinflammation in autism spectrum disorders." J Neuroinflammation 9 (2012): 265.
[4] Rossignol, D. A., et al. "Evidence linking oxidative stress, mitochondrial dysfunction, and inflammation in the brain of individuals with autism." Frontiers in physiology 5 (2014).
[5] Teunissen, C. E., et al. "Inflammation markers in relation to cognition in a healthy aging population." Journal of neuroimmunology 134.1 (2003): 142-150.
[6] Sorce, S., et al. "NOX enzymes in the central nervous system: from signaling to disease." Antioxidants & redox signaling 11.10 (2009): 2481-2504.
[7] Hernandes, M. S., et al. "The role of Nox2-derived ROS in the development of cognitive impairment after sepsis." Journal of neuroinflammation 11.1 (2014): 36.
[8] Newey, S. E., et al. "Rho GTPases, dendritic structure, and mental retardation." Journal of neurobiology 64.1 (2005): 58-74.
[9] Kasri, N. N., and Linda Van Aelst. "Rho-linked genes and neurological disorders." Pflügers Archiv-European Journal of Physiology 455.5 (2008): 787-797.
[10] Chong CM, et al. "Discovery of a benzofuran derivative (MBPTA) as a novel ROCK inhibitor that protects against MPP^+-induced oxidative stress and cell death in SH-SY5Y cells." Free Radical Biology and Medicine 74 (2014) :283-293.
[11] Miyano, K., et al. "Direct involvement of the small GTPase Rac in activation of the superoxide-producing NADPH oxidase Nox1." Journal of Biological Chemistry 281.31 (2006): 21857-21868.
[12] Stanley, A., et al. "Rho GTPases and Nox dependent ROS production in skin. Is there a connection?." Histology and histopathology 27.11 (2012): 1395-1406.
[13] Glide, version 5.7, Schrödinger, LLC, New York, NY, 2011.
[14] Therese, P. J., et al. "Multiple e-Pharmacophore Modeling, 3D-QSAR, and High-Throughput Virtual Screening of

Hepatitis C Virus NS5B Polymerase Inhibitors." Journal of chemical information and modeling 54.2 (2014): 539-552.

[15] Hawkins, Paul CD, A. Geoffrey Skillman, and Anthony Nicholls. "Comparison of shape-matching and docking as virtual screening tools." Journal of medicinal chemistry 50.1 (2007): 74-82.

[16] Doran, et al. "ROCK Enzymatic Assay." Wnt Signaling. Humana Press, 2008. 197-205.

[17] Niesen, et al. "The use of differential scanning fluorimetry to detect ligand interactions that promote protein stability." Nature protocols 2.9 (2007): 2212-2221.

[18] Buttke, et al. "Use of an aqueous soluble tetrazolium/formazan assay to measure viability and proliferation of lymphokine-dependent cell lines." Journal of immunological methods 157.1 (1993): 233-240.

[19] Das, et al. "Mangiferin attenuates methylmercury induced cytotoxicity against IMR-32, human neuroblastoma cells by the inhibition of oxidative stress and free radical scavenging potential." Chemico-biological interactions 193.2 (2011): 129-140.

[20] Eruslanov, Evgeniy, et al. "Identification of ROS using oxidized DCFDA and flow-cytometry." Advanced Protocols in Oxidative Stress II. Humana Press, 2010. 57-72.

[21] Puck, Theodore T., et al. "A rapid method for viable cell titration and clone production with HeLa cells in tissue culture: the use of X-irradiated cells to supply conditioning factors." Proceedings of the National Academy of Sciences of the United States of America 41.7 (1955): 432.

[22] Liang, et al. "In vitro scratch assay: a convenient and inexpensive method for analysis of cell migration in vitro." Nature protocols 2.2 (2007): 329-333.

[23] Bunn, Robert C., et al. "Palmitate and insulin synergistically induce IL-6 expression in human monocytes." Cardiovascular diabetology 9.1 (2010): 73.

[24] Yoza B. K., et al. "Interleukin-1beta expression after inhibition of protein phosphatases in endotoxin-tolerant cells." Clin Diagn Lab Immunol. 1998, 5, 281.

[25] Moran, C. J., et al. "Expression and modulation of Rho kinase in human pregnant myometrium." Molecular human reproduction 8.2 (2002): 196-200.

[26] Lin, P. C., et al. "Collapsin response mediator proteins (CRMPs) are a new class of microtubule-associated protein (MAP) that selectively interacts with assembled microtubules via a taxol-sensitive binding interaction." Journal of Biological Chemistry 286.48 (2011): 41466-41478.

[27] Ago, T., et al. "Nox4 as the major catalytic component of an endothelial NAD (P) H oxidase." Circulation 109.2 (2004): 227-233.

[28] Shen M, et al. "Discovery of Rho-kinase inhibitors by docking-based virtual screening." Molecular Biosystems. 9.6 (2013):1511-1521.

[29] Shen M, et al. "Discovery and optimization of triazine derivatives as ROCK1 inhibitors: molecular docking, molecular dynamics simulations and free energy calculations." Molecular Biosystems 9.3(2013):361-374

[30] Pan P, et al. "Advances in the development of Rho-associated protein kinase (ROCK) inhibitors." Drug Discovery Today 18 (2013):1323-1333.

[31] Battu M. B., et al. "Pharmacophore-Based 3D QSAR and Molecular Docking Studies to Identify New Non-Peptidic Inhibitors of Cathepsin S". Current Medicinal Chemistry. Sep 17 (2013) Epub ahead of print

[32] Street, C. A., et al. "Pharmacological inhibition of Rho-kinase (ROCK) signaling enhances cisplatin resistance in neuroblastoma cells." International journal of oncology 37.5 (2010): 1297.

[33] Fujimura, M., et al. "Inhibition of the Rho/ROCK pathway prevents neuronal degeneration in vitro and in vivo following methylmercury exposure." Toxicology and applied pharmacology 250.1 (2011): 1-9.

[34] Fujimura, M., et al. "Methylmercury exposure downregulates the expression of Racl and leads to neuritic degeneration and ultimately apoptosis in cerebrocortical neurons." Neurotoxicology 30.1 (2009): 16-22.

[35] Franken, N. A. P., et al. "Clonogenic assay of cells in vitro." Nature protocols 1.5 (2006): 2315-2319.

[36] Pantoliano, M. W., et al. "High-density miniaturized thermal shift assays as a general strategy for drug discovery." Journal of biomolecular screening 6.6 (2001): 429-440.

[37] Wyckoff, J. B., et al. "ROCK-and myosin-dependent matrix deformation enables protease-independent tumor-cell invasion in vivo." Current Biology 16.15 (2006): 1515-1523.

[38] Ogata, S., et al. "Fasudil inhibits lysophosphatidic acid-induced invasiveness of human ovarian cancer cells." International Journal of Gynecological Cancer 19.9 (2009): 1473-1480.

[39] Kim, S. Y., et al. "Role of NADPH oxidase-2 in lipopolysaccharide-induced matrix metalloproteinase expression and cell migration." Immunology and cell biology 88.2 (2009): 197-204.

[40] Prosser, B. L., et al. "X-ROS signaling: rapid mechano-chemo transduction in heart." Science 333.6048 (2011): 1440-1445.

[41] Simon, F., et al. "Early lipopolysaccharide-induced reactive oxygen species production evokes necrotic cell death in human umbilical vein endothelial cells." Journal of hypertension 27.6 (2009): 1202-1216.

[42] Kim, H. J., et al. "Roles of NADPH oxidases in cisplatin-induced reactive oxygen species generation and ototoxicity." The Journal of neuroscience 30.11 (2010): 3933-3946.

[43] Matoba, K., et al. "Rho-kinase mediates TNF-α-induced MCP-1 expression via p38 MAPK signaling pathway in mesangial cells." Biochemical and biophysical research communications 402.4 (2010): 725-730.

Journal Name RSCPublishing

ARTICLE

Sr.No	NOX2 (LPS stimulated U87MG)				Rhokinase				HEK Cell lines	MeHg treated IMR32	SI (CC50/GIC50)	Clonogenic Assay (IMR32)		
	H bond	Glide g score	Docking score	X-ROS IC50(μM)	H bond	Glide g score	Docking score	ROCK IC50(μM)	CC50(μM)	GIC50 (μM)		No.of colonies	PE	SF
1	4	-5.147	-4.226	13.93	2	-6.45	-7.377	0.001848	1.15	33.470	0.03	35	35	1.22
2	3	-6.639	-6.32	3.304	3	-5.65	-5.973	0.001588	64.46	2.232	28.87	52	52	2.70
3	5	-8.404	-8.079	2.853	3	-6.02	-6.351	0.001879	428.2	0.003031	141273	76	76	5.77
4	3	-7.828	-7.589	10.75	3	-6.11	-6.349	0.002301	20.41	0.720	28.34	45	45	2.02
5	6	-7.825	-7.812	0.7923	4	-7.39	-7.41	0.00412	1.359	0.165	8.21	67	67	4.48
6	4	-7.431	-7.413	8.794	2	-6.28	-6.299	0.02158	16.02	1.374	11.65	46	46	2.11
7	5	-9.029	-8.753	1.037	1	-7.05	-7.334	0.01744	41.78	16.97	2.46	58	58	3.36
Fasudil	NA	NA	NA	NA	2	-8.28	-8.286	0.8562	3.836	0.01771	216.60	56	56	3.13

Table2: Designed 7 compounds docking score and glide g score, Invitro enzyme activity and cell line activity data in comparison with ROCK1 inhibitor Fasudil.

Journal Name

RSCPublishing

ARTICLE